Simultaneous Visualization of Hydrogen Peroxide and Water Concentrations Using Photofragmentation Laser-Induced Fluorescence

Larsson, Kajsa; Aldén, Marcus; Bood, Joakim

Published in:
Applied Spectroscopy

DOI:
10.1177/0003702817702386

2017

Document Version:
Peer reviewed version (aka post-print)

Kajsa Larsson, Marcus Aldén, and Joakim Bood

Simultaneous Visualization of Hydrogen Peroxide and Water Concentrations Using Photofragmentation Laser-Induced Fluorescence

Applied Spectroscopy (Volume 71, Issue Number 9), pp. 2118 – 2127

http://journals.sagepub.com/doi/10.1177/0003702817702386

Simultaneous visualization of H_2O_2 and H_2O concentrations using photofragmentation laser-induced fluorescence

Kajsa Larsson, Marcus Aldén and Joakim Bood*

Div. of Combustion Physics, Lund University, Box 118, 221 00 Lund, Sweden

*Author to whom correspondence should be addressed

E-mail: joakim.bood@forbrf.lth.se

Abstract

A concept based on photofragmentation laser- induced fluorescence (PFLIF) is for the first time demonstrated for simultaneous detection of hydrogen peroxide (H_2O_2) and water (H_2O) vapor in various mixtures containing the two constituents in a bath of argon gas. A photolysis laser pulse at 248 nm dissociates H_2O_2 into OH fragments, whereupon a probe pulse, delayed 100 ns and tuned to an absorption line in the $A^2\Sigma^+$ (v=1) ← $X^2\Pi$ (v=0) band of OH near 282 nm, induces fluorescence. The total OH fluorescence reflects the H_2O_2 concentration, while its spectral shape is utilized to determine the H_2O concentration via a model predicting the ratio between the fluorescence intensities of the $A^2\Sigma^+$ (v=1) → $X^2\Pi$ (v=1) and the $A^2\Sigma^+$ (v=0) → $X^2\Pi$ (v=0) bands. The H_2O detection scheme requires that the bath gas has a collisional cross section with OH(A) that is significantly lower than that of H_2O, which is the case for argon. Spectrally dispersed OH fluorescence spectra were recorded for five different H_2O_2/H_2O/Ar mixtures; the H_2O_2 concentration ranging from 30 to 500 ppm and the H_2O concentration ranging from 0 to 3%. Fluorescence intensity ratios predicted by the model for these mixtures agree very well with corresponding experimental data, which thus validates the model. The concept was also demonstrated for two-dimensional imaging, using two intensified CCD cameras for signal detection. Water content was here sensed through the different temporal characteristics of the two fluorescence bands by triggering the two cameras so that one captures the total OH fluorescence while the other one captures only the early part, which mainly stems from $A^2\Sigma^+$ (v=1) → $X^2\Pi$ (v=1) fluorescence. Hence the H_2O_2 concentration is reflected by the image of the camera recording the total OH fluorescence, whereas H_2O concentration is extracted from the ratio between the two camera images. Quantification of the concentrations was carried out based on calibration measurements performed in known mixtures of H_2O_2 (30 – 500 ppm) and H_2O (0 – 3%) in bulk argon. The detection limits for single-shot imaging are estimated to be 20 ppm for H_2O_2 and 0.05% for

H_2O. The authors believe that the concept provides a valuable asset in, for example, pharmaceutical or aseptic food packaging applications, where H_2O_2/H_2O vapor is routinely used for sterilization.

Keywords: photofragmentation, laser-induced fluorescence, imaging, hydrogen peroxide, water

1. Introduction

Hydrogen peroxide (H_2O_2) is a molecule of great importance in several scientific fields, particularly atmospheric and combustion chemistry, but also in many practical applications. Hydrogen peroxide is for example commonly used as sterilization agent in aseptic food packaging, pharmaceutical engineering, and spacecraft systems. For a thorough description of key activation mechanisms, organic functional group oxidations, and a review of a large range of applications, see the book by Jones.[1] In most vapor-phase H_2O_2 applications the vapor is generated from an aqueous H_2O_2 solution. In aseptic food packaging, for example, typically a liquid mixture containing 35 wt-% H_2O_2 and 65 wt-% H_2O, is evaporated, brought into contact with a hot gas stream, and fed into the volume to be sterilized.[2] Thus, both H_2O_2 and H_2O are present in the volume, making simultaneous detection of both species of great interest.

In terms of measurement techniques, laser-based methods possess a number of advantageous properties, such as allowing non-intrusive measurements *in situ* with high spatial and temporal resolution. Some laser-based techniques provide two-dimensional (2-D) imaging if the laser beam is formed into a sheet and the generated signal is recorded with a 2-D detector such as a CCD camera. As already alluded to, development of *in-situ* measurement techniques for detection of gas-phase H_2O_2 and H_2O is strongly motivated, mainly due to the large number of industrial applications involving mixtures of the two species. The two species are often chemically linked to each other, making simultaneous detection of particular interest. However, rather few studies, where the two species are measured simultaneously, have been carried out. Corveleyn *et al.*[3] and Adams *et al.*[4] have reported simultaneous detection using near-infrared (NIR) absorption spectroscopy for monitoring vapor concentrations. H_2O_2 and H_2O have spectrally overlapping absorption lines in the near infrared region. Adams *et al.*[4] extracted the water concentration directly from the absorbance

of 1362 nm, while the hydrogen peroxide concentration was extracted from 1422 nm with corrections for the overlap of water vapor absorption. H_2O_2 and H_2O mole fractions was estimated in an HCCI engine, using wavelength-agile absorption spectroscopy by Hagen and Sanders.[5] Furthermore, extracting absolute concentrations in absorption-based measurement techniques are beneficial since quenching and predissociation not have to be considered. A drawback is, however, that they are line of sight techniques, and are restricted to measurement volumes in which concentration and temperature variations along the line of sight are insignificant.

Laser induced- fluorescence (LIF) is a laser based technique able to visualize flow patterns in two dimensions to compare experimental measurements with 2-D simulations. Given that the exciting laser beam is formed into a sheet, planar laser induced fluorescence (PLIF) has 2-D measurement capacity. Water vapor has electronic transitions in the vacuum-ultraviolet (VUV) spectral region requiring multi photon excitation for 2D visualization with PLIF. A method that potentially can extract both temperature and H_2O concentration in flames was presented by Pitz *et al.*,[6] who studied 2-photon fluorescence spectra in a hydrogen/air flame, using a tunable KrF excimer laser (248 nm). 2-D measurements of water vapor in flames was demonstrated by Neij *et al.*[7] They also used 2-photon LIF for single shot visualization of water vapor in a hydrogen/air diffusion flame under engine-like conditions and report a 0.2% detection limit for their case.

Hydrogen peroxide lacks bound excited electronic states in the UV-visible region causing difficulties for direct LIF detection. However H_2O_2 can be measured indirectly by a pump-probe concept called photofragmentation laser-induced fluorescence (PFLIF). A UV-laser pulse first photodissociates the H_2O_2 molecule into two OH fragments, whereupon a probe laser pulse, tuned to an absorption line of OH, induces fluorescence, whose intensity is related to the H_2O_2 concentration. The PFLIF technique for H_2O_2 has been demonstrated for 2-D

measurements under ambient conditions,[8] but also in various fields such as combustion diagnostics and for sterilization of food packages.[9] For combustion diagnostics H_2O_2 has been visualized both in flames[10] and in an HCCI engine[11] using PFLIF. In all these areas the concept was demonstrated using a frequency-quadrupled Nd:YAG laser for photolysis and a frequency-doubled dye laser for probing of OH fragments. The choice of photolysis laser is not critical as long as the wavelength is short enough to dissociate the H_2O_2 molecule into OH fragments. However, since the absorption cross section increases with decreasing wavelength,[12] it is preferable to use a photolysis beam in the UV region.

In a recent study, Larsson and coworkers demonstrated a concept for simultaneous detection of H_2O_2 and H_2O based on a combination of PFLIF (for H_2O_2) and 2-photon LIF (for H_2O).[13] A tunable injection-locked KrF excimer laser (248 nm) was employed both for H_2O_2 photolysis and 2-photon excitation of H_2O. It was found that the sensitivity for H_2O detection was limited due to poor collimation characteristics of the excimer laser beam, preventing efficient focusing of the beam, which is critical for the 2-photon LIF signal as it depends on the square of the laser intensity. Furthermore, the squared laser intensity dependence also has a negative impact on the shot-to-shot variations of the H_2O fluorescence.

In the present work a new technique for simultaneous measurement of H_2O_2 and H_2O is proposed and demonstrated. The basis of the method is still PFLIF, based on UV photolysis followed by OH LIF with excitation in the $A^2\Sigma^+$ (v=1) ← $X^2\Pi$ (v=1) band, and the total OH fragment-fluorescence intensity reflects the H_2O_2 concentration. Extraction of H_2O concentration, however, is based on the fact that the ratio between OH fragment fluorescence emitted in the 1-1 and 0-0 band is dependent on the H_2O content. The dynamics between the two fluorescence bands is strong, i.e. the H_2O sensitivity is high, when the surrounding medium, i.e. the bath gas, has a low cross section for collisional quenching. In order to demonstrate the concept, measurements were carried out in different mixtures of vaporized

H_2O_2/H_2O in argon bath gas. Based on a spectroscopic study it was confirmed that a model for the H_2O-dependent ratio between fluorescence in the 1-1 and 0-0 band well predicts the experimental ratios. Since the spectral shape is dependent on molecular collisions, the temporal shape of the OH fluorescence is dependent on the H_2O concentration as well. This feature is utilized in imaging experiments, where two gated intensified CCD cameras are employed. One camera has a short gate, capturing only the early part of the fluorescence signal, while another camera has a longer gate capturing the entire fluorescence signal. The ratio between the two camera images thus provides a 2-D map of the H_2O concentration, while the image recorded with the camera having the longer gate reflects the H_2O_2 concentration. It is demonstrated that the method is capable of providing simultaneous single-shot images of H_2O_2 and H_2O concentration distributions, which makes the measurement concept interesting for a number of applications, for example in optimizing sterilization of food packages, where the evaporation of aqueous H_2O_2 solutions is critical.[14,15]

2. Photophysics and model

The PFLIF concept is schematically illustrated in Fig. 1. First a UV pump pulse dissociates the H_2O_2 molecule into two OH fragments, whereupon a probe pulse, tuned to an OH absorption line, excites the OH fragments, which upon deexcitation emit fluorescence. The fluorescence intensity is proportional to the number density of OH fragments and thereby the concentration of H_2O_2.

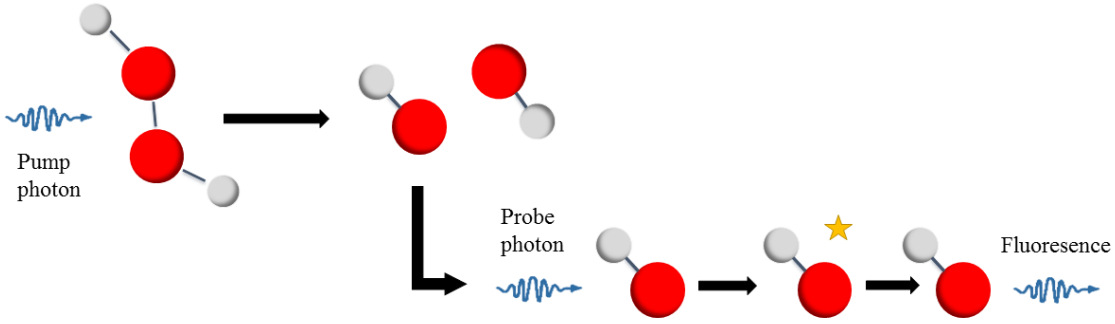

Fig. 1 *Schematic illustration of the PFLIF concept. First a pump photon dissociates the H_2O_2 molecule into two OH fragments, whereupon a probe photon excites the OH fragment, inducing emission of fluorescence.*

Energy levels and transitions relevant for the probing of OH fragments are shown in Fig. 2. With the probe laser tuned to a resonant transition in the $A^2\Sigma^+$ (v'=1) ← $X^2\Pi$ (v''=0) band, fluorescence can be emitted from both the directly pumped vibrational level, v'= 1, and from v'= 0 following vibrational energy transfer (*VET*).

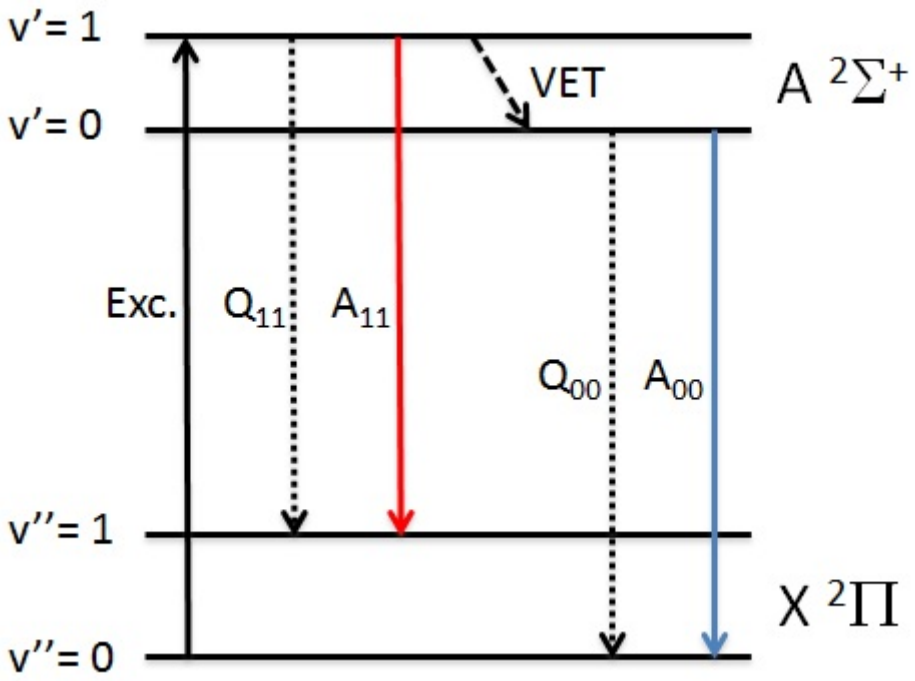

Fig. 2 *Energy level diagram of the relevant OH transitions. The abbreviation Exc. designates excitation, VET vibrational energy transfer, Q_{11} and Q_{00} quenching, and A_{11} and A_{00} Einstein coefficients for spontaneous emission.*

The quantum yield for fluorescence in the 1-1 band is given by the expression

$$\phi_{11} = \frac{A_{11}}{A_{11}+Q_{11}+VET} \ , \tag{1}$$

where A_{11} is the Einstein coefficients for spontaneous emission in the 1-1 band and Q_{11} is the quenching rate in the 1-1 band. The quantum yield for fluorescence in the 0-0 band is given by

$$\phi_{00} = \frac{VET}{A_{11}+Q_{11}+VET} \cdot \frac{A_{00}}{A_{00}+Q_{00}} \ , \tag{2}$$

where A_{00} is the Einstein coefficients for spontaneous emission in the 0-0 band and Q_{00} is the quenching rate in the 0-0 band. Now, the ratio between the two fluorescence quantum yields can be expressed as in Eq. (3), given that $A_{00} << Q_{00}$, which a good approximation at atmospheric pressure regardless of composition.

$$\frac{\phi_{11}}{\phi_{00}} \approx \frac{A_{11}}{A_{00}} \cdot \frac{Q_{00}}{VET} \ , \tag{3}$$

In the current study, the probe volume consists of H_2O/H_2O_2 vapor in argon bath gas. The H_2O_2 concentration is, however, too low (<600 ppm) to have significant impact on quenching and vibrational energy transfer, and its contribution to these processes is therefore neglected. If we let the variable x designate the mole fraction of H_2O, Q_{00}, Q_{11}, and VET can be written:

$$Q_{00}(x) = N_{tot}[q_{Ar}^0 \cdot (1-x) + q_{H2O}^0 \cdot x] \tag{4}$$

$$Q_{11}(x) = N_{tot}[q_{Ar}^1 \cdot (1-x) + q_{H2O}^1 \cdot x] \tag{5}$$

$$VET(x) = N_{tot}[k_{Ar} \cdot (1-x) + k_{H2O} \cdot x] \ , \tag{6}$$

where q_{Ar}^0 and q_{H2O}^0 are quenching rate constants for argon and H_2O, respectively, for v' = 0, $q_{Ar}^1$and q_{H2O}^1 the corresponding constants for v' = 1, and k_{Ar} and k_{H2O} are vibrational energy

transfer (VET) rate constants for argon and H_2O, respectively. N_{tot} is the total number density of the gas ($2.49 \cdot 10^{19}$ cm^{-3} at 295 K). Substituting (4) and (6) into (3) thus results in the following expression:

$$\frac{\phi_{11}}{\phi_{00}} = \frac{A_{11}}{A_{00}} \cdot \frac{q_{Ar}^0 \cdot (1-x) + q_{H2O}^0 \cdot x}{k_{Ar} \cdot (1-x) + k_{H_2O} \cdot x} \quad . \tag{7}$$

Since the only variable in Eq. (7) is x, it is possible to directly determine the H_2O concentration by measuring the ratio between the fluorescence band intensities, which can be done in the spectral domain, either using a spectrograph or a spectral filter, where the latter alternative allows 2-D imaging.

Another alternative is to utilize that the temporal shape of the OH fluorescence signal is dependent on the water concentration. The fluorescence emitted in the two bands, i.e. F_{11} and F_{00}, are proportional to the populations in v'=1 and v' = 0, respectively. The time-dependent populations in these two states, $N_1(t)$ (population in v' = 1) and $N_0(t)$ (population in v' = 0), can be found by solving the following differential equations:

$$\frac{dN_1}{dt} = -(Q_{11} + A_{11} + VET)N_1 \tag{8a}$$

$$\frac{dN_0}{dt} = VET \cdot N_1 - (Q_{00} + A_{00})N_0 \, , \tag{8b}$$

with the initial conditions $N_1(0) = n$ and $N_0(0) = 0$, i.e. n molecules are in v'=1, while v' = 0 is empty at t = 0. The fluorescence intensities emitted in the two bands can then be written:

$$F_{11}(t,x) = n \cdot A_{11} e^{-(Q_{11}(x) + A_{11} + VET(x))t} \tag{9a}$$

$$F_{00}(t,x) = n \cdot A_{00} \cdot \frac{VET(x)}{A_{00} - A_{11} - VET(x)} \cdot \left[e^{-(Q_{11}(x) + A_{11} + VET(x))t} - e^{-(Q_{00}(x) + A_{00})t} \right]. \tag{9b}$$

Summation of the two contributions thus yields the total emitted fluorescence:

$$F_{tot}(t,x) = n \cdot \left[A_{00} e^{-Q_{00}(x)t} + (A_{11} - A_{00}) e^{-(Q_{11}(x) + VET(x))t} \right] \tag{10}$$

The expression is based on the assumption that both the quenching and VET rates are much larger than the spontaneous emission rates, which is the case in the present study.

3. Experimental arrangement

An injection-locked KrF excimer laser (Lambda Physik, EMG 150 MSC), emitting laser pulses of 248 nm wavelength and ~0.2 cm^{-1} linewidth (full width at half maximum, FWHM) at a repetition rate of 10 Hz, was used to photodissociate H_2O_2. The laser pulse energy was ~150 mJ and the pulse duration was ~17 ns (FWHM). A frequency-doubled dye laser (Quantel, TDL-90), operating with a Rh 590/ethanol dye solution, was tuned to 281.91 nm in order to induce fluorescence from OH photofragments by exciting the overlapping $Q_1(1)$ and $R_2(3)$ transition of the $A^2\Sigma^+$ (v=1) ← $X^2\Pi$ (v=0) absorption band in OH. The dye laser was pumped by a frequency-doubled Nd:YAG laser (Quantel, YG981-E10) with 10-Hz pulse repetition rate. The UV laser pulses generated by the dye laser had a duration of ~8 ns (FWHM), a linewidth of ~0.1 cm^{-1} (FWHM), and pulse energy of ~7 mJ. The dye laser was fired 100 ns after the excimer laser in order to ensure that the OH fragments had attained thermal equilibrium at the time of the arrival of the 282-nm probe pulse.[8]

A schematic description of the experimental setup is illustrated in Fig. 3. The two beams were spatially overlapped using a dichroic mirror, which is highly reflective at 248 nm and highly transmitting at 282 nm. In order to make sure that OH fragments were probed in the linear fluorescence regime, the 282-nm beam was left unfocused with a diameter of 6 mm. However, in order to retain spatial resolution, the 248-nm beam was focused with a cylindrical lens (CL) of focal length 400 mm, forming a vertical laser sheet with a height of 6 mm and thickness ~600 μm, having its center 10 mm above the outlet (10 mm inner diameter) of the bubbler flask.

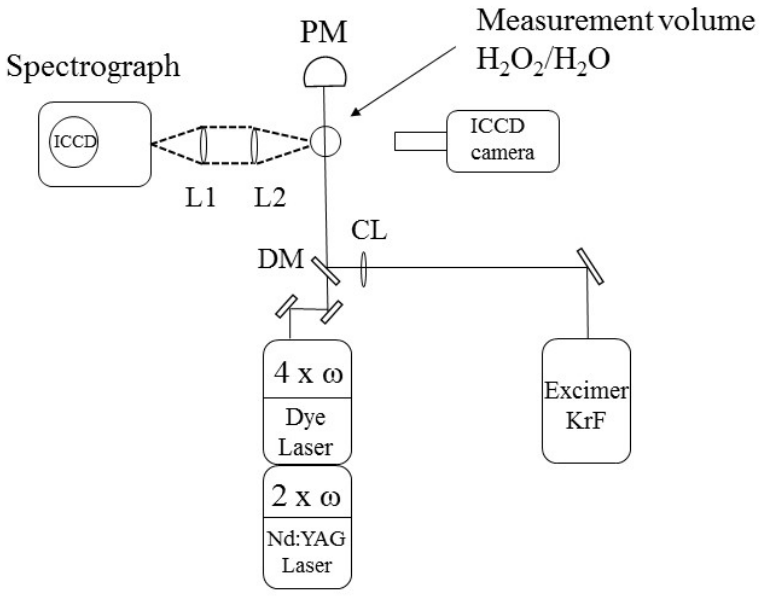

Fig. 3 *Schematic description of the experimental setup. Abbreviations; DM: Dichroic mirror, CL: cylindrical lens (f =400 mm), L1: spherical lens (f=200 mm), L2: spherical lens (f=150 mm), and PM: power meter.*

The OH fluorescence could be monitored spectrally dispersed, using a 0.5-m spectrograph (Princeton Instruments, Acton Model SP-2556) equipped with an intensified CCD camera (Princeton Instruments, PI-MAX 3). The OH fluorescence is first collected with a spherical lens of 200-mm focal length (L2) and then focused onto the entrance slit of the spectrograph using a spherical lens with a focal length 150 mm (L1). The spectrograph was oriented such that its entrance slit became parallel with the laser beam propagation direction. The spectrograph had a grating with 1200 grooves/mm (blazed at 300 nm) and the width of the entrance slit was 50 µm.

Two intensified CCD cameras were used in the imaging studies (both Princeton Instruments, PI-MAX 2), one of them located as outlined in Fig. 3. In these studies the spectrograph and its collection optics were removed to make room for the second CCD camera. The camera intensifiers (microchannel plates, MCPs) allow gated detection and the two cameras were triggered so that one of them only monitors the early part of the fluorescence signal (approximately 10 ns), while the other camera captures the entire

fluorescence signal (50 ns). A pulse/delay generator (SRS, DG535) was used for synchronization of laser pulses and cameras. A WG 305 (3 mm thick) Schott filter was positioned in front of each camera in order to suppress scattered laser light.

Different H_2O_2/H_2O/Ar gas mixtures were established in the probe volume by bubbling argon through different H_2O_2/H_2O mixtures contained in a bubbler flask. Liquid concentrations and the resulting vapor concentrations are summarized in Table 1.

Table 1 *Liquid and gaseous H_2O_2/H_2O concentrations used in the experiments.*

Liquid concentrations (wt-%)		**Vapor concentrations**	
H_2O_2	**H_2O**	**H_2O_2 (ppm)**	**H_2O (%)**
0	100	0	2.7
10	90	29	2.45
20	80	83	2.3
30	70	163	2.02
40	60	271	1.7
50	50	425	1.43

All solutions except the 30/70 and 50/50 wt-% liquid mixtures were prepared by diluting a 50/50 wt-% H_2O_2/H_2O solution with deionized water. The 30/70 and 50/50 solutions were stock solutions from Sigma Aldrich, used without preparatory treatment. The gas-phase H_2O_2 and H_2O concentrations were calculated from partial vapor pressures tabulated by Schumb *et al.*[16] using the temperature 295 K, which was the temperature measured in the laboratory air. The vapor pressure is strongly temperature dependent and, hence, the temperature in the laboratory was continuously monitored during the experiments.

4. Result and discussion

4.1 Spectroscopic investigation

Figure 4 shows a comparison between an experimental fluorescence spectrum (a), recorded in a mixture containing 425 ppm H_2O_2 and 1.4% H_2O in argon bath gas, and a simulated OH

fluorescence spectrum (b). The calculated spectrum was simulated using LIFBASE[17]. The two emission bands, i.e. the 0-0 band, ranging from 306 to 312 nm, and the 1-1 band, ranging from 312 to 318 nm, are clearly visible and the experimental and simulated spectra agree very well.

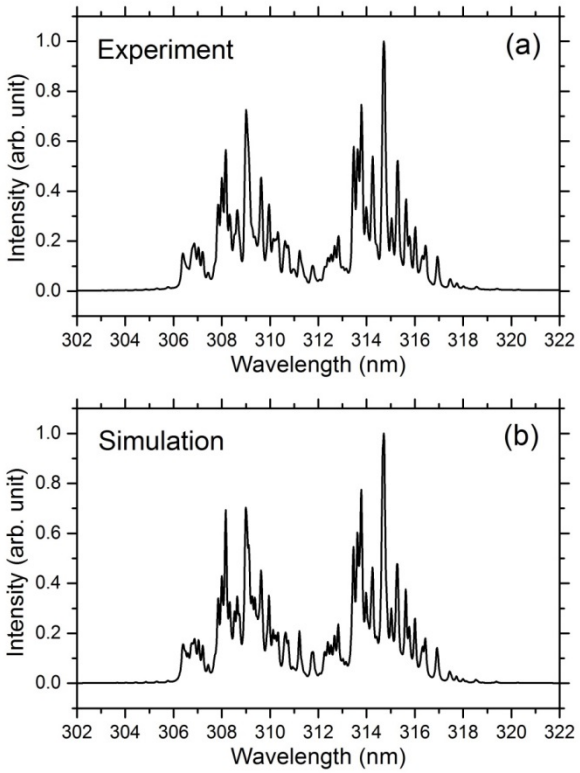

Fig. 4 *Experimental (a) and simulated (b) OH fragment fluorescence spectrum. The experimental spectrum was recorded in a mixture containing 425 ppm H_2O_2 and 1.4% H_2O in argon bath gas at 295 K.*

Figure 5 displays the rotational population distributions in v' = 1 (a) and v' = 0 (b) used to create the simulated spectrum shown in Fig. 4b. The rotational distribution in v' = 1 (a), i.e. the directly pumped vibrational state, is assumed to be thermal and has been set to 295 K. For v'= 0 the rotational population distribution was fitted and the distribution shown in (b) resulted in the best agreement between the simulated and experimental spectrum (see Fig. 4). As evident from Fig. 5b, VET from v' = 1 to v' = 0 puts significant population in high

rotational states, giving rise to a rotationally hot distribution in v' = 0, which is consistent with previous observations.[18]

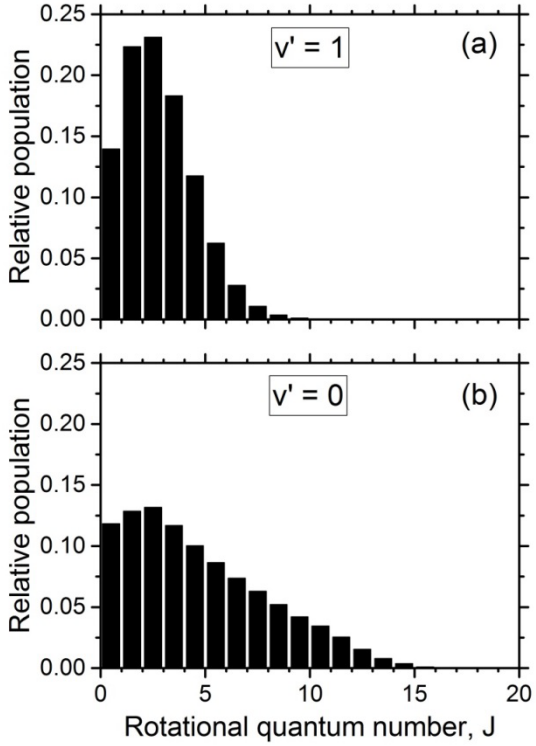

Fig. 5 *Rotational population distributions in v' = 1 (a) and v' = 0 (b) used to simulate the spectrum shown in Fig. 4b.*

Fluorescence spectra were recorded for five different H_2O_2/H_2O/Ar mixtures of known compositions. The total fluorescence intensity was determined for each gas mixture by integrating the fluorescence signal from 305 to 320 nm, and the resulting intensities are indicated by solid square symbols in the diagram shown in Fig. 6. The data points show a slight non-linear dependence on the H_2O_2 concentration. The reason for the deviation from linear dependence is due to the fact that the H_2O concentration decreases, i.e. the fluorescence quantum yield increases, with increasing H_2O_2 concentration. Fluorescence quantum yields were therefore calculated for the five different compositions using Eqs. (1) and (2) with input from Eqs. (4) – (6). The following rate constants were used for the calculations: q^0_{Ar} = $5.0\cdot10^{-13}$ cm^3/s,[19] q^0_{H2O} = $6.28\cdot10^{-10}$ cm^3/s,[20] q^1_{Ar} = $3.4\cdot10^{-13}$ cm^3/s,[21] q^1_{H2O} = $5.9\cdot10^{-10}$ cm^3/s,[22] k_{Ar} = $4.1\cdot10^{-12}$ cm^3/s,[18] k_{H2O} = $7.3\cdot10^{-11}$ cm^3/s,[18] A_{00} = $1.45\cdot10^6$ s^{-1},[17] and A_{11} =

$8.68 \cdot 10^5$ s^{-1}.[17] Values on the v'=0 quenching rate constants for water, q^0_{H2O}, are only available for the rotational states N= 0, 3, 5, and 7, and the value used here is for N = 7. The reason for using this value, rather than the thermal value ($q_{H2O} = 7.26 \cdot 10^{-10}$ cm^3/s [20]), which is based on only low rotational states, is to better account for the thermally hot rotational population observed in v'=0 (see Fig. 5b).

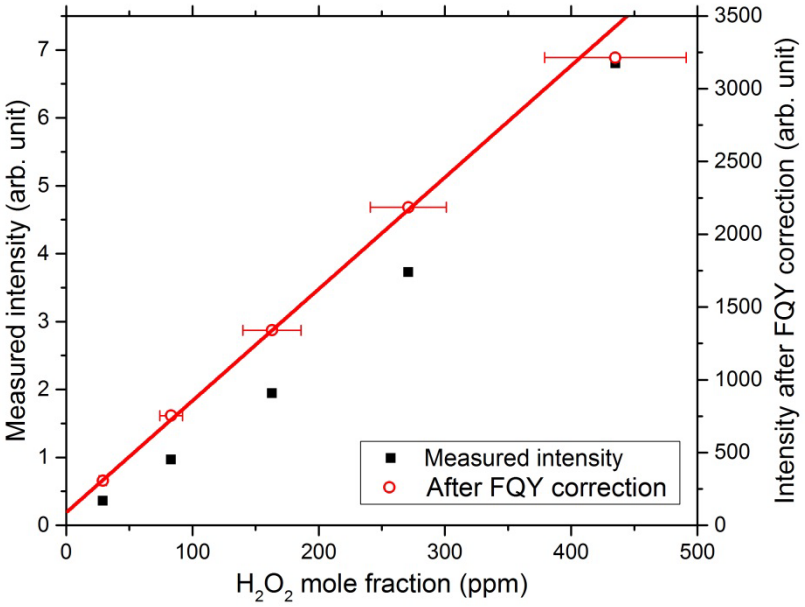

Fig. 6 *Measured fluorescence intensity vs H_2O_2 concentration (solid squares). The open circles indicate data obtained by division with the corresponding fluorescence quantum yield (FQY) and the solid line is a linear fit to these data points.*

Using the calculated fluorescence quantum yields, the data points were corrected by dividing the measured intensities with the corresponding fluorescence quantum yield, as indicated by the red open circles in Fig. 6. Errors in the concentrations of the liquid mixtures are estimated to ±1% and the liquid temperature is assumed to be accurate to within ±1 K. Uncertainties in vapor-phase H_2O_2 concentrations due to these inaccuracies are indicated by the error bars. A weighted fit (weight factors $w_i = 1/\sigma_i^2$, where σ_i is the error bar) of a linear function to the corrected data points resulted in the solid line shown in the figure. The corrected data nicely follow the linear function within the current experimental uncertainty. The fitted line intercepts the ordinate slightly above zero, suggesting that some OH is

produced even when H_2O_2 is absent, i.e. through photodissociation of H_2O. However, the energy of a 248-nm photon is not high enough to reach the lowest repulsive state of H_2O,[23] which thus rules out single-photon dissociation. It has been shown that OH can be produced by 2-photon dissociation (248 nm), however, this production channel is expected to be insignificant in comparison with OH production through (single-photon) dissociation of H_2O_2.[13]

To illustrate the influence of the water concentration, x, on the spectral shape of the OH fragment fluorescence, normalized experimental spectra (highest signal set to unity) for three of the investigated gas mixtures are displayed in Fig. 7. As can be seen, the intensity in the 0-0 relative to the 1-1 band is decreasing with increasing water concentration.

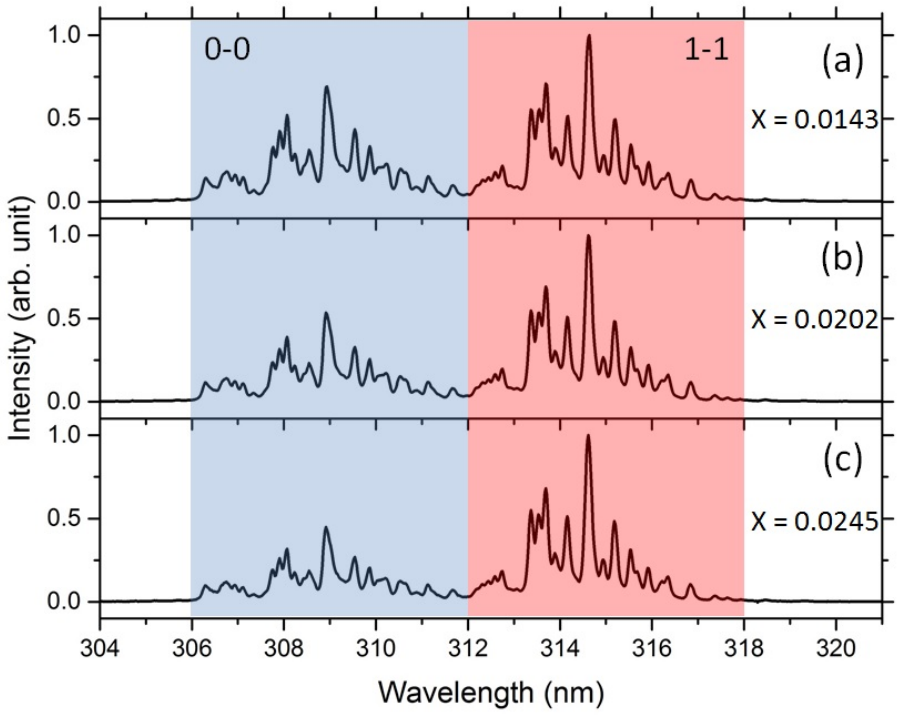

Fig. 7 *Normalized OH fragment fluorescence spectra at 295 K for the H_2O mole fractions x = 0.0143 (a), 0.0202 (b), and 0.0245 (c). The corresponding H_2O_2 concentrations were 435 ppm (a), 163 ppm (b), and 29 ppm (c). The spectral regime corresponding to the two emission bands have been shaded in blue (0-0) and red (1-1).*

The ratio between the integrated intensity emitted in the 1-1 band (312-318 nm), F_{11}, and the integrated intensity in the 0-0 band (306-312 nm), F_{00}, was calculated for the five different

gas mixtures. Ratio versus H_2O concentration is plotted in the diagram shown in Fig. 8. The experimental data (open symbols) agree very well with ratios calculated using Eq. (7) (black solid line). Using Eq. (7), but with q_{Ar}^0 and k_{Ar} replaced by the corresponding constants for nitrogen (q_{N2}^0 = 3.6·10^{-11} cm^3/s [20] and k_{N2} = 2.3·10^{-10} cm^3/s [18]) and air (q_{air}^0 = 5.5·10^{-11} cm^3/s [20] and k_{air} = 1.9·10^{-10} cm^3/s [18]), ratio vs H_2O mole fraction was also calculated for air and nitrogen, respectively, and the results are illustrated by the blue dashed line (air) and the red dotted line (nitrogen) in Fig. 8. As can be seen, these curves are virtually flat, indicating that the band-intensity ratio is essentially independent of the H_2O content in the current concentration interval for these bath gases. The reason for the large difference in H_2O sensitivity for argon in comparison with air and nitrogen is mainly because the latter two bath gases have ~50 times higher VET rate constants than argon, which makes the impact of H_2O on the rate insignificant.

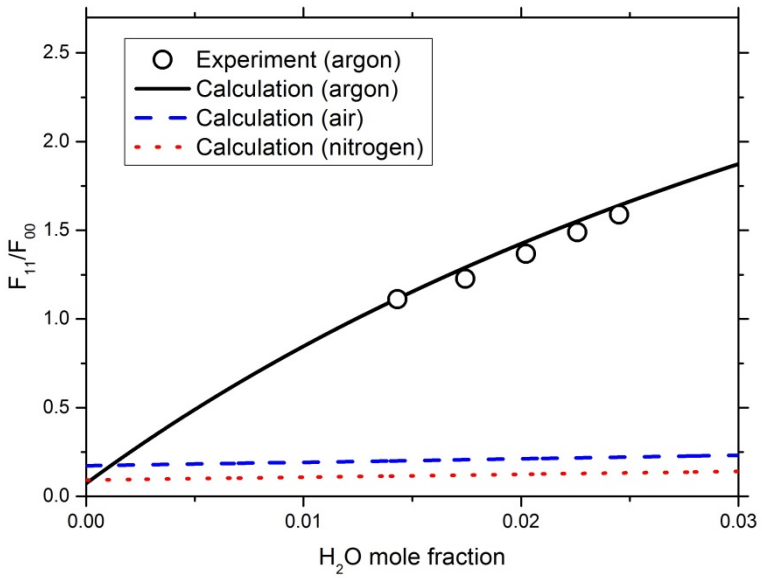

Fig. 8 *Measured band intensity ratio, F_{11}/F_{00}, vs H_2O concentration. The black line is calculated using Eq. (7) assuming argon bath gas, while the red line is the corresponding calculated curve for air as bath gas. The H_2O_2 concentrations corresponding to the data points range from 29 to 435 ppm.*

In order to predict how the concept for H_2O measurement might work in for example hot sterilization or other processes where the H_2O concentrations are expected to be significantly higher than in the present study, the band-intensity ratio, F_{11}/F_{00}, was calculated for H_2O mole fractions ranging from 0 to 1 (assuming argon bath gas), using Equation (7) and the same quenching and VET constants as previously. The result is shown in Fig. 9. As can be seen, the method provides high sensitivity for H_2O concentrations between 0 and 10%. Beyond 10% concentration the curve levels off and becomes virtually flat for concentrations higher than 50%.

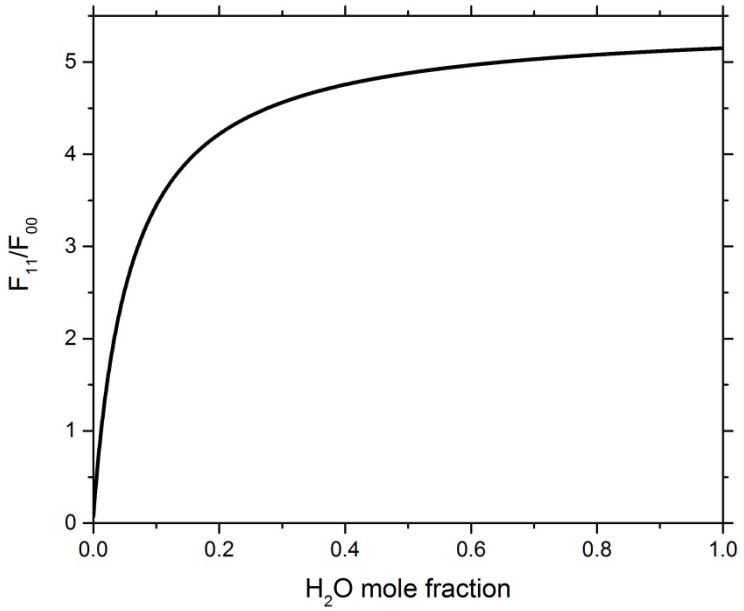

Fig. 9 *Band-intensity ratio calculated using Equation (7) for H_2O mole fractions ranging from 0 to 1 with argon as bath gas. The quenching and VET constants used in the calculations are the same as used for the calculations presented in Fig. 8, i.e. they are valid for 295 K.*

4.2 Demonstration of 2-D imaging

The spectroscopic investigation, reported in the previous section, strongly suggests that simultaneous imaging of H_2O_2, through the total OH fluorescence intensity, and H_2O, through the band-intensity ratio, is feasible. Emission in the two bands, i.e. 0-0 and 1-1 obviously needs to be distinguished, which can be done using a spectral filter with a very sharp transmission edge at 312 nm. However, it is also possible to extract H_2O concentration by

sensing the temporal shape of the fluorescence, since it is dependent on the H_2O concentration (x), as evident from Eq. (10). Since the fluorescence is induced by a laser pulse of a certain temporal shape, the fluorescence given by Eq. (10) should, thus, be convoluted with the temporal profile of the laser pulse. Assuming a Gaussian laser pulse with 8 ns FWHM, fluorescence signals for six different water concentrations are calculated, and the results are shown in Fig. 10a. To emphasize how the shape of the signal depends on the H_2O concentration, the signals have been normalized so that their maxima are at unity. As can be seen, the fluorescence lifetime decreases monotonically with increasing H_2O concentration.

Since we are aiming at 2-D single-shot imaging based on gated detection using two ICCD cameras, the fluorescence signals, shown in Fig. 6a, were integrated from -10 to 5 ns, yielding the area $S_{short}(x)$, and from -10 to 70 ns, yielding the area $S_{long}(x)$. The ratio $S_{short}(x)/S_{long}(x)$ as a function of x, i.e. the H_2O concentration, is plotted in the diagram shown in Fig. 10b. As can be seen in the figure, the ratio is strongly dependent of the H_2O concentration, ranging from 0.07 at zero H_2O concentration to 0.76 at 3% concentration. A comparison with Fig. 8 reveals that utilizing the temporal characteristics provides roughly the same sensitivity to variations in H_2O concentration as the method based on the spectral characteristics of the fluorescence.

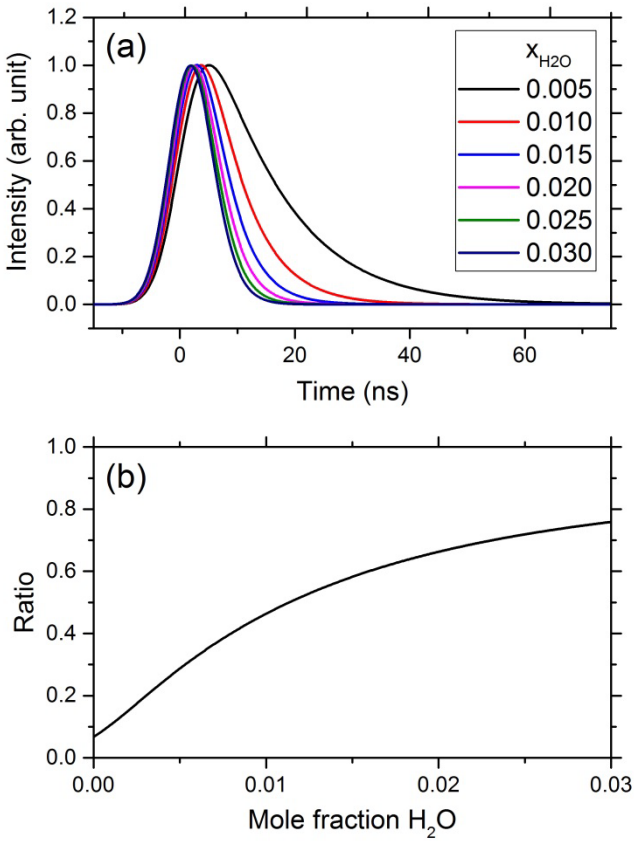

Fig. 10 *(a) Normalized fluorescence signals calculated using Eq. (10). (b) The ratio S_{short}/S_{long} vs H_2O concentration. The temperature is assumed to be 295 K.*

The measurement concept was demonstrated experimentally for simultaneous 2-D imaging of H_2O_2 and H_2O. The intensifier on Camera 1 was triggered so that only the early part of the fluorescence signal was recorded, i.e. S_{short}, while the other camera (Camera 2) collected the entire fluorescence, i.e. S_{long}. Pixels were binned 2×2 on both cameras. The image recorded by Camera 2 reflects the H_2O_2 concentration, while the ratio between the two camera images, i.e. S_{short}/S_{long} reflects the H_2O concentration. The timing for closure of the gate on Camera 1 had to be determined empirically, based on both the sensitivity to H_2O concentration, manifested by the ratio S_{short}/S_{long}, and adequate signal-to-noise ratio. Since camera gate functions typically are far from perfect top-hat profiles,[24] the point in time corresponding to the falling edge of the gate of Camera 1 is uncertain, but as a rough estimate this camera detected signal during the initial 10 ns of the signal. With the camera parameters

finally set, calibration measurements were performed in the aforementioned mixtures of known H_2O_2/H_2O/Ar concentrations.

Simultaneous single-shot 2-D imaging of H_2O_2 and H_2O in a volume containing a H_2O_2/H_2O concentration gradient was then demonstrated. The concentration gradient was created by issuing two adjacent gas jets of different H_2O_2/H_2O concentrations into the probe volume. The two jets were created using two separate bubbler flasks, containing two different liquid H_2O_2/H_2O mixtures, through which argon gas was bubbled. The two gaseous mixtures were flowing from the bubbler flasks towards the measurement volume in separate Teflon tubes (4 mm inner diameter). Close to the measurement volume the two Teflon tubes were put directly next to each other so that two gas jets – one with ~0.016 H_2O and ~450 ppm H_2O_2 and the other with ~0.023 H_2O and ~150 ppm H_2O_2 – were issued straight up into still air. The lower edge of the 6-mm high vertical laser sheets was located ~3 mm above the outlets of the Teflon tubes. The resulting H_2O_2 concentration image is shown in Fig. 11a and the corresponding image of the H_2O concentration is displayed in Fig. 11b. Quantitative concentrations, as indicated by the two color bars, were extracted using the calibration measurements. Both images have been smoothed through a median filter (8x8), resulting in a resolution of 0.7 mm/pixel. The image quality is lower in the H_2O image (b) than in H_2O_2-image (a), mainly due to the fact that the former image is a result of dividing two images, increasing the noise in quadrature, which in particular enhances edge artifacts. Therefore the concentration gradient present between the two jet flows is more clearly observed in the H_2O_2 image (a). The detection limits for single-shot imaging are estimated to be 20 ppm for H_2O_2 and 0.05% for H_2O with the present resolution.

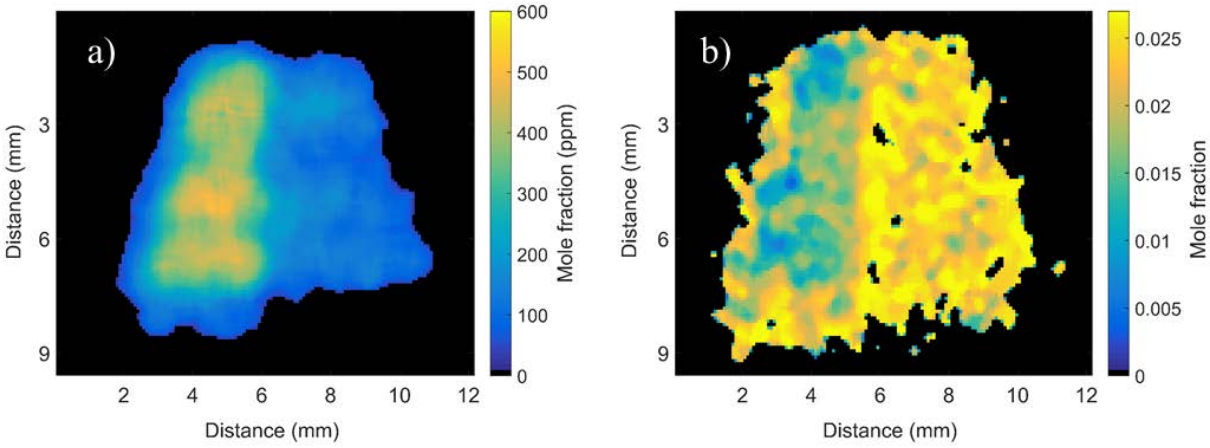

Fig. 11 *Simultaneously recorded single-shot images of H_2O_2 (a) and H_2O concentration (b). The composition (mole fraction) of the left jet was ~0.016 H_2O and ~450 ppm H_2O_2, while the right jet carried ~0.023 H_2O and ~150 ppm H_2O_2. The temperature was 295 K.*

With the camera gate functions thoroughly characterized, these functions can be included in the model, allowing quantification of the H_2O concentration without calibration. In addition optimum gate timings can be determined more accurately from modeling results, as described in Ref. 24. A major improvement is anticipated if the dual-imaging and modelling approach, demonstrated by Ehn *et al.*,[24,25] is implemented in a setup based on picosecond laser excitation. Whether an approach based on the spectral band intensity ratio would be better than the temporal approach is essentially a question about which filter is the sharpest, i.e. a spectral filter (with transmission edge at 312 nm) or a temporal edge filter provided by the rising or falling slope of a camera gate. If the two filters are equally sharp, our simulations suggest that the sensitivities should be similar (compare Figs. 8 and 10b).

5. Conclusions

Photofragmentation laser-induced fluorescence has been demonstrated for simultaneous detection of hydrogen peroxide (H_2O_2) and water (H_2O) in various mixtures containing the two constituents and argon bath gas. The H_2O_2 concentration is determined from the total fluorescence signal from the OH fragments produced by UV-laser photolysis of H_2O_2, while

the water concentration is extracted by measuring the intensity ratio between the fluorescence in the 1-1 and 0-0 emission bands or by sensing the temporal shape of the total fluorescence signal. Experimentally measured band-intensity ratios agree very well with calculated ratios based on quenching and VET rate constants found in the literature. Simultaneous single-shot imaging of H_2O_2 and H_2O is successfully demonstrated using a setup where the temporally early part and the total fluorescence signal are detected by separate ICCD cameras. The detection limits for single-shot imaging are estimated to 20 ppm and 0.05%, for H_2O_2 and H_2O, respectively. Although the measurement concept requires a bath gas possessing weak collisional deactivation of OH $A^2\Sigma^+(v=1)$, such as argon, the authors believe that it should be of interest in for example pharmaceutical or aseptic food packaging applications, where H_2O_2/H_2O vapor is routinely used for sterilization.

Acknowledgement

The authors would like to thank the Swedish Energy Agency (Energimyndigheten) for financial support through the Center for Combustion Science and Technology (CECOST). Funding through the ERC Advanced Grant TUCLA is also gratefully acknowledged. We also would like to thank Tetra Pak Packaging Solutions, for providing necessary equipment, and Malin Jonsson, Elin Malmqvist, Dina Hot, and Olof Johansson, for fruitful discussions as well as technical assistance.

References

1. C.W. Jones. Applications of Hydrogen Peroxide and Derivatives. J.S. Clark, editor. The Royal Society of Chemistry, 1999.
2. S. Radl, S. Ortner, R. Sungkorn, J.G. Khinast. “The engineering of hydrogen peroxide decontamination systems”. J. Pharm. Innov. 2009. 4(2): 51–62.
3. G.M.R.V. S. Corveleyn, J.P.Remon. “Near-Infrared (NIR) Monitoring of H_2O_2 Vapor Concentration During Vapor Hydrogen Peroxide (VHP) Sterilisation”. Pharm. Res. 1997. 14(3): 294–298.
4. D. Adams, G.P. Brown, C. Fritz, T.R. Todd. “Calibration of a near-infrared (NIR) H_2O_2 vapor monitor”. Pharm. Eng. 1998. 18(3): 1–11.
5. C.L. Hagen, S.T. Sanders. “Investigation of multi-species (H_2O_2 and H_2O) sensing and thermometry in an HCCI engine by wavelength-agile absorption spectroscopy”. Meas. Sci. Technol. 2007. 18(7): 1992–1998.
6. R.W. Pitz, T.S. Cheng, J.A. Wehrmeyer, C.F. Hess. “Two-photon predissociative fluorescence of H_2O by a KrF laser for concentration and temperature measurement in flames”. Appl. Phys. B Photophysics Laser Chem. 1993. 56(2): 94–100.
7. H. Neij, M. Aldén. “Application of two-photon laser-induced fluorescence for visualization of water vapor in combustion environments.” Appl. Opt. 1994. 33(27): 6514–6523.
8. O. Johansson, J. Bood, M. Aldén, U. Lindblad. “Detection of hydrogen peroxide using photofragmentation laser-induced fluorescence”. Appl. Spectrosc. 2008. 62(1): 66–72.
9. O. Johansson. Development and application of photofragmentation laser-induced fluorescence for visualization of hydrogen peroxides. PhD thesis, LRCP-143, Lund University, 2011.
10. O. Johansson, J. Bood, B. Li, A. Ehn, Z.S. Li, Z.W. Sun, et al. “Photofragmentation laser-induced fluorescence imaging in premixed flames”. Combust. Flame. 2011. 158(10): 1908–1919.
11. B. Li, M. Jonsson, M. Algotsson, J. Bood, Z.S. Li, O. Johansson, et al. “Quantitative detection of hydrogen peroxide in an HCCI engine using photofragmentation laser-induced fluorescence”. Proc. Combust. Inst. 2013. 34(2): 3573–3581.
12. C.L. Lin, N.K. Rohatgi, W.B. DeMore. “Ultraviolet absorption cross sections of hydrogen peroxide”. Geophys. Res. Lett. 1978. 5(2): 113–115.
13. K. Larsson, O. Johansson, M. Aldén, J. Bood. “Simultaneous visualization of water and hydrogen peroxide vapor using two-photon laser-induced fluorescence and photofragmentation laser-induced fluorescence”. Appl. Spectrosc. 2014. 68(12): 1333–1341.
14. C. Hultman, A. Hill, G. McDonnell. “The physical chemistry of decontamination with gaseous hydrogen peroxide”. Pharm. Eng. 2007. 27(1): 22.
15. B. Unger-Bimczok, V. Kottke, C. Hertel, J. Rauschnabel. “The influence of humidity, hydrogen peroxide concentration, and condensation on the inactivation of geobacillus stearothermophilus spores with hydrogen peroxide vapor”. J. Pharm. Innov. 2008. 3(2): 123–133.
16. W.C. Schumb, C.N. Satterfield, R.L. Wentworth. Hydrogen peroxide. Reinhold Publishing Corporation, New York, 1955.
17. J. Luque, D.R. Crosley. LIFBASE: Database and Spectral Simulation Program. SRI International Report MP 99-009, 1999.
18. L.R. Williams, D.R. Crosley. “Collisional vibrational energy transfer of OH ($A\ ^2\Sigma^+$, $v'=1$)”. J. Chem. Phys. 1996. 104(17): 6507–6014.
19. K.H. Becker, D. Haaks, T. Tatarczyk. “The natural lifetime of OH($^2\Sigma^+$, v=0, N=2,

J=3/2) and its quenching by atomic hydrogen". Chem. Phys. Lett. 1974. 25(4): 564–567.
20. R.A. Copeland, M.J. Dyer, D.R. Crosley. "Rotational-level-dependent quenching of A $^2\Sigma^+$ OH and OD". J. Chem. Phys. 1985. 82(1985): 4022–4032.
21. P. Hogan, D.D. Davis. "Electronic quenching and vibrational relaxation of the OH (A $^2\Sigma^+$, v′=1) state". J. Chem. Phys. 1975. 62(11): 4574–4576.
22. R.A. Copeland, M.L. Wise, D.R. Crosley. "Vibrational energy transfer and quenching of hydroxyl ($A^2\Sigma^+$, v' = 1)". J. Phys. Chem. 1988. 92(20): 5710–5715.
23. H. Okabe. Photochemistry of Small Molecules. John Wiley and Sons, New York, 1978.
24. A. Ehn, O. Johansson, A. Arvidsson, M. Aldén, J. Bood. "Single-laser shot fluorescence lifetime imaging on the nanosecond timescale using a Dual Image and Modeling Evaluation algorithm." Opt. Express. 2012. 20(3): 3043–3056.
25. A. Ehn, M. Jonsson, O. Johansson, M. Alde. "Quantitative oxygen concentration imaging in toluene atmospheres using Dual Imaging with Modeling Evaluation". Exp Fluids. 2013. 54: 1433.